A new space instrumental concept based on dispersive components for the measurement of CO2 concentration in the atmosphere

(MicroCarb Mission)

PASCAL Veronique, BUIL Christian, CANSOT Elodie, LOESEL Jacques, TAUZIEDE Laurie, PIERANGELO Clemence, BERMUDO François
Centre National d'Etudes Spatiales (CNES),
Toulouse – France
veronique.pascal@cnes.fr

OLIVIER Mathieu
ALTEN Sud Ouest
Toulouse, France

DUBREUIL Mickael
SOPHIA CONSEIL
Toulouse, France

***Abstract*— Measuring the concentration of greenhouse gases from space is a current challenge. This measurement is achieved via a precise analysis of the signature of chemical gaseous species (CO_2, CH_4, CO, etc.) in the spectrum of the reflected sunlight. First at all, two families of spectrometers have been studied for the MicroCarb mission. The first family is based on the phenomena of interference between two radiation waves (Michelson Interferometer). The second family is based on the use of dispersive optical components. The second family has been selected for the forthcoming studies in the MicroCarb project. These instruments must have high radiometric and spectral resolutions, in narrow spectral bands, in order to discriminate between absorption lines from various atmospheric chemical species, and to quantify their concentration. This is the case, for example, for the instrument onboard the OCO-2 satellite (NASA/JPL).**

Our analysis has led us to define a new instrumental concept, based on a dispersive grating spectrometer, with the aim of providing the same accuracy level as the OCO-2, but with a more compact design for accommodation on the Myriade Evolution microsatellite class. This compact design approach will allow us to offer a moderate-cost solution to fulfil mission objectives. Two other studies based on dispersive grating are in progress by CNES prime contractors (ASTRIUM and THALES ALENIA SPACE).

A summary of the main specifications of this design will be described, in particular the approach with the so-called "merit function". After a description of such a space instrument, which uses a specific grating component, a preliminary assessment of performances will be presented, including the theoretical calculations and formula. A breadboard implementation of this specific grating has allowed us to show the practicality of this concept and its capabilities. Some results of this breadboard will be described. In addition, an instrument simulator is being developed to validate the performances of this concept. A grating component prototype has been built, and the specifications, together with the expected performances, will be described, in particular the polarisation ratio. Some elements about detectors will be also given regarding their suitability for the mission. This preliminary design is encouraging and shows that such a spectrometer may be compatible with a microsatellite platform (low mass, low power and compact design). Some prospects of improvements will also be considered.

Keywords: MicroCarb, infrared spectrometer, dispersive grating, greenhouse gases concentration, spatial instrument

I. INTRODUCTION

The MicroCarb mission is designed to measure the carbon dioxide (CO_2) column to within 1 ppm (a measurement accuracy of some 0.3%) from a space observatory in low earth orbit (LEO) so as to locate and characterise CO_2 sinks in order to better understand the carbon cycle and predict its evolution.

The absorption lines of carbon dioxide gas lie in the SWIR (Short Wave InfraRed) band. The MicroCarb mission therefore intends to measure the spectral radiance of solar radiation reflected by the earth at the nadir over land and through glint over oceans (Level 1). These spectral radiance measurements will be converted into column-integrated CO_2 concentrations to provide geophysical products (Level 2) which will be converted into surface fluxes by an inversion algorithm that takes into account a transport model. The resulting products are called Level 4 products. The measurement itself is made within discrete sounding points representing on the earth a surface area of several square kilometres. The mission's measurement accuracy is driven by the tiny variability in the CO_2 column, variations being around +/-1 ppm out of 380ppm.

The measurement principle is based on the inversion of the spectral content of the area sounded. The instrument observes the earth's atmosphere through three very narrow spectral windows. Its basic task is to accurately measure the spectral radiance reaching the top of the atmosphere (TOA) (Fig.1). The light analysed is from the sun, once bounced back off the earth's surface at the targeted sounding point and absorbed by atmospheric gases—including CO_2—and possibly scattered by atmospheric aerosols.

Carbon dioxide gas has absorption lines in the thermal infrared at 1.6 µm (band B2) and 2.0 µm (band B3). The sun's radiation at these wavelengths, reflected by the earth back to the satellite, therefore contains the molecule's signature. It is the depth of the absorption lines that contains the information on CO_2 concentration. An additional spectral band in the oxygen band at 0.76 µm, noted band B1, provides surface pressure data on spectrum inversion. This band also provides information on the contribution of atmospheric aerosols and fine clouds to the radiation collected by the onboard instrument. Data from this third band are taken into account when the CO_2 spectra are inverted to enhance accuracy.

Above land, the satellite acquires measurements with a nadir line of sight. Above oceans, water being dark in the near-infrared and therefore not reflecting sunlight in a lambertian way, MicroCarb will aim at the glint, i.e. the sun's specular reflectance. This capability of following the glint enables a large enough flux to be obtained at the instrument entrance, thus allowing atmospheric CO_2 concentration to be measured above oceans.

The observation system is complemented by a two-dimensional imaging function at a wavelength of 0.76 µm to observe the sounded area. This 2D map of the sounded field accompanies each item of spectral data acquired by the instrument, and will provide data upon clouds.

The instrument must be able to operate with the required accuracy aboard a Myriade Evolution satellite bus.

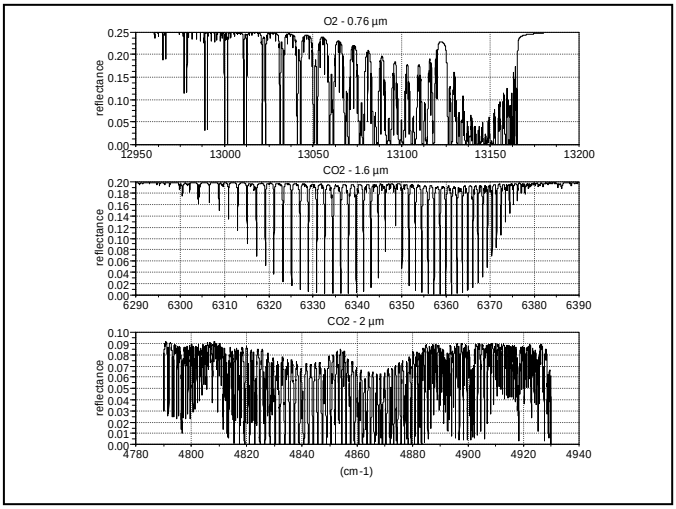

Figure 1. Typical TOA reflectance spectra

For MicroCarb, an initial phase 0 focused on an instrument concept using a grating spectrometer to meet mission needs and the necessity to fly the instrument on a Myriade microsatellite bus. Grating spectrometer is the case, for example, of the instrument aboard NASA's Orbiting Carbon Observatory (OCO) [1]. The main results of this preliminary in-house CNES research project, to be described below, appears sufficiently credible to pursue this dispersive instrument concept. An invitation to tender was initiated to study two types of instrument concepts: a static Fourier transform concept and a dispersive grating concept (whatever the type of dispersive element: prism, échelle grating, immersive grating). One of the objectives of MicroCarb Phase A is to select the best of the two instrument concepts meeting mission requirements. Design activities are divided into three by the chosen manufacturers, Thales Alenia Space and Astrium:

- initial phase A1 from February 2011 to September 2011, when the two specified instrument concepts were subjected to a comparative analysis covering different criteria such as feasibility, performance, scheduling and cost. The choice made by CNES relied on the outputs of the industry satellite and instrument studies as well as on the evaluations of the performances of CO_2 and fluxes retrievals accuracies. A grating spectrometer instrumental concept with 3 spectral bands (0.76 µm (B1), 1.6µm (B2) and 2.0 µm (B3)) has been formally selected for the Micrcarb mission.
- second phase A2 from September 2011 to February 2012, when the chosen instrument concept was consolidated and preliminary design : performance budgets and satellite budgets, for instance, were completed.
- third phase A3 from June 2012 to March 2013, is devoted to the technological pre-development and characterisation of critical devices for mission performances or feasibility as gratings, polariser devices...

The MicroCarb Phase A will be concluded by mid 2013 with a Preliminary Requirements Review (PRR).

In addition to these satellite activities with Astrium and Thales Alenia Space, complementary activities initiated during this phase A will also be performed by CNES during the coming 2012 and 2103 period. Some of them are described in this paper.

II. SPECTROMETER DESCRIPTION

A. General principle

This part describes the spectrometer studied at CNES which was based on a dispersive optical element: the échelle grating spectrometer [2].

The instrument is divided into three parts; see Fig. 2:

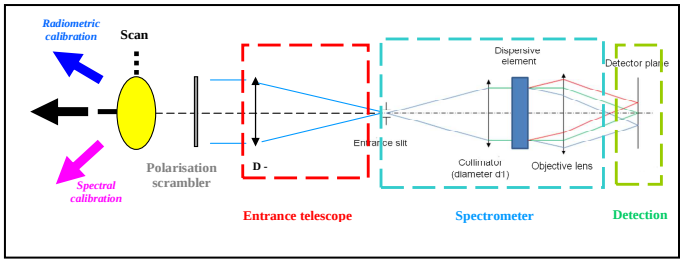

Figure 2. Components of the instrument's functional system

- The entrance telescope which collects fluxes along a given line of sight and forms a sharp image of the earth at the spectrometer entrance. An scan mirror and a polarisation scrambler can be put before the telescope.

- The spectrometer itself, which analyses incoming light by breaking it down into its different spectral components for projection onto a detector array.

- A focal plane with the detectors and electronics.

The field of view at the entrance of the instrument's spectrometer section is limited by a physical slit. The spectrometer forms sharp monochromatic images of this slit on three matrix detector array. The three detectors are associated with the three spectral bands: B1 (0.76 microns), B2 (1.6 microns) and B3 (2.05 microns). These spectral bands are relatively narrow, but are observed with a high-power resolution, typically R = 25000 ($R = \lambda/\Delta\lambda$, where $\Delta\lambda$ is the spectral width at half transmission along a monochromatic spectral line).

Using a long slit provides a spatial dimension on each detector which is perpendicular to the direction of spectral scattering. The information acquired along this axis can be added together (binning) to increase radiometric resolution. Typically, 50 pixels (Nbin) are summed in this way (Fig.3). The long axis of the slit is itself approximately perpendicular to the movement of the satellite at the nadir. Fig. 3 illustrates this geometric configuration and the terminology used in this case.

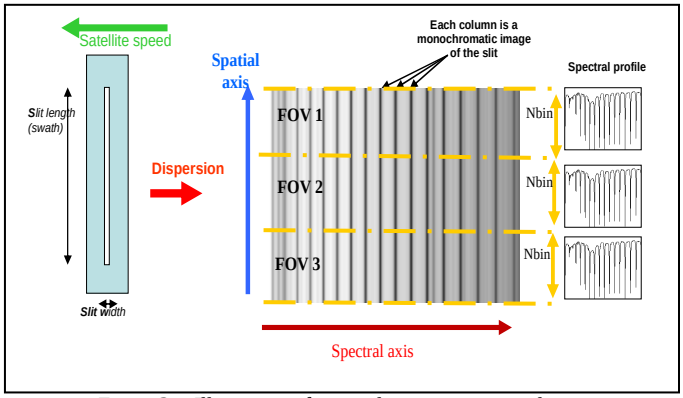

Figure 3. Illustration of spectral axis versus spatial axis

The spectrometer must have a high-power resolution within a restricted space. It is known that the power resolution of a grating spectrometer used in near Littrow conditions is described by one of the following equations (1) or (2):

$$R = \frac{\lambda\, k\, m\, d1}{\phi\, D \cos\alpha} \qquad (1)$$

$$R = \frac{2\ \ d1 \tan\alpha}{\phi\, D} \qquad (2)$$

Where:

D= diameter of the entrance telescope

ϕ = angular width of the slit in radians

α = angle of incidence on the grating

d1 = diameter of the spectrometer's internal pupil (linked to spectrometer size)

k = diffraction order

m = density of etched grooves

Diameter *d1* is necessarily small due to the size issue. The value of entrance pupil diameter *D* is determined by the radiometric resolution. The spectral power resolution for a given instrument volume will therefore be optimised by increasing the angle of incidence α, diffraction order number *k*, or groove density *m*.

One of the fundamental characteristics of the MicroCarb instrument is its compactness, because it has to fly on a Myriade Evolution microsatellite bus. For this reason, we chose an optical concept based on double pass Tri Mirror Anastigmat (TMA) or Four-Mirror Anastigmat (FMA). Double pass means that the same optical components are used for the collimation function (light rays are made parallel before they arrive at the dispersive component) and for the camera lens function (the rays dispersed by the dispersive component are focused on the focal plane). The addition of a fourth mirror allows an additional degree of freedom to improve the quality image without increasing the size of the instrument. An initial implementation of this concept (see fig. 4) has been studied, taking into account a calibration system and active and/or passive thermal control. The volume is compatible with that available on a Myriade Evolution bus (H: 412mm x w: 700 mm x L: 864mm).

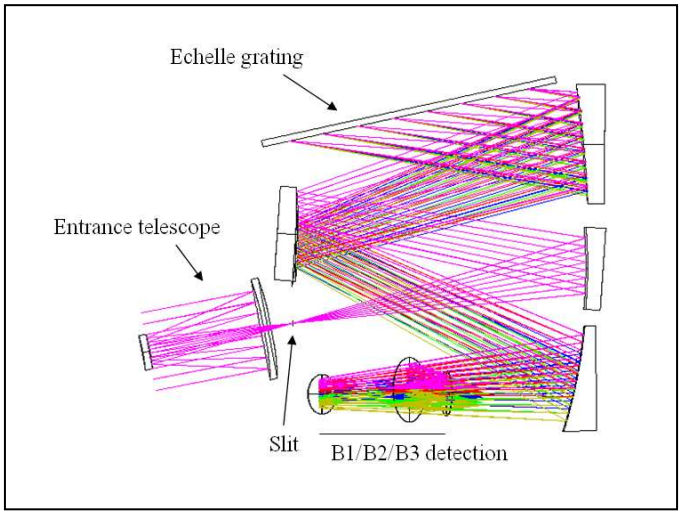

Figure 4. Typical optical configuration. The diffraction orders for the desired spectral bands are separated and sent to the corresponding detectors by a set of dichroic filters.

B. Zoom on dispersive component: echelle grating

This part describes the main component of the spectrometer studied at CNES: the echelle grating.

Spectral coverage requirements (bands B1, B2 and B3) led us to favour an increased incidence angle and diffraction order to the detriment of groove density. The type of grating with these characteristics is known as an "echelle" grating. This kind of component allows spectral multiplexing. By carefully choosing the grating parameters, central wavelengths of spectral bands can coincide with optimal echelle grating diffraction efficiency in specific diffraction orders. To further increase performance, the echelle grating is operated in near-Littrow conditions, i.e. the diffraction angle at the diffraction peak is nearly identical to the angle of incidence of rays on the grating. Using a high diffraction order ($13 < k < 50$) along with a carefully selected pitch m can provide diffracting combinations in the same directions as the rays associated with the centre of bands B1, B2 and B3.

Useful information is distributed in distinct diffraction orders, so the signal carried by these orders must be separated so it can be sent to each detector optimised for one band (B1, B2 and B3).

Conventionally, diffraction orders in an echelle spectrometer are physically separated through a slightly dispersive auxiliary element functioning perpendicularly to the main dispersive element (cross disperser). We rejected this solution because we are only interested in a relatively small number of spectral bands at the same time, these bands being covered by distinct diffraction orders. The orders are separated by a set of dichroic filters and spectral bandpass filters centred on the bands of interest (Fig. 4). As previously seen, the characteristics of the grating are carefully chosen so that the diffraction angle is identical for the central wavelength of each band.

The separation of diffraction orders by the echelle grating through bandpass filters is well-suited to the use of a long slit, which maximises instrument scope.

The main features of the echelle grating are as shown in table 1 below:

TABLE I. ECHELLE GRATING CHARACTERISTICS

Spectral bands	B1	B2	B3
Diffraction order	35 for B1	17 for B2	13 for B3
Size	48 mm along the lines and 140 mm perpendicularly to the lines		
Groove density	69.33 lines/mm		
Blaze angle	67.9°		

C. Experimentation of the instrument principle

We set up an experiment to trial the principle of an echelle grating spectrometer operating in MicroCarb's spectral bands. This breadboard uses a standard (Richardson) echelle grating. The assembly was calculated and set up so as to attain a power resolution of up to R = 40000 in the CO_2 1.6 micron band (i.e. a spectral width of 0.04 nanometres, see Fig.5).

Fig.6 shows the simplified optical configuration used for this feasibility breadboard. The equipment can be used to check the principle behind order selection through bandpass filters, measure the polarimetric specifications of gratings, specify the processing and calibration algorithms, and enhance the modelling of this kind of instrument

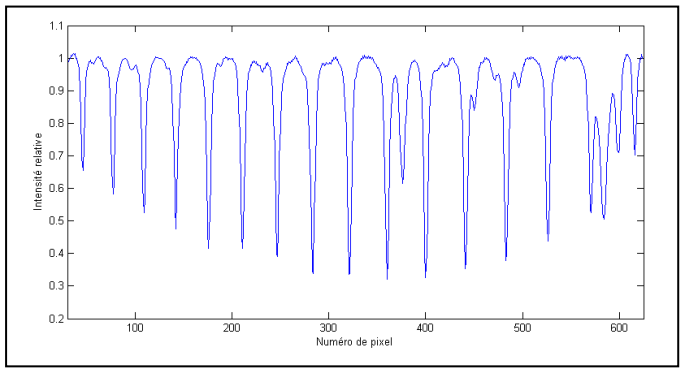

Figure 5. Example of an experiment profile for the CO2 spectrum in band B2 (uncalibrated)

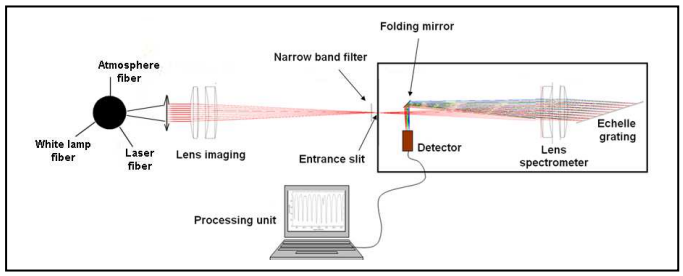

Figure 6. MicroCarb Engineering Breadboard

III. Main Performance requirements and assessment

A. Parametric relationship (level 1)

The level 1 requirements for MicroCarb instrument are such that:

- the goal gives the same level 2 performance as OCO [3]
- The threshold is such that Level 2 performance is relaxed by 35%.

The signal/noise ratio, spectral resolution and bandwidth are the instrument's driving parameters for CO2 retrieval accuracy. As very different combinations of these parameters might give similarly good Level 2 performance, we define a parametric relationship:

$$p = \frac{k}{BW^{\alpha} SNR^{\beta} R^{\gamma} N^{\delta} M^{\delta}}$$

Where:
k =coefficient set such that p is equal to the required performance in ppm calculated through linear error estimates [4] for a clear sky without aerosols.
BW = spectral bandwidth
SNR = signal to noise ratio
R = spectral resolution
N = number of across-track FOV
M= number of along-track FOV
$\alpha, \beta, \gamma, \delta$ are optimal values fitted for a set of different instrument configurations.

The requirements asks p to below 0.4 (goal) or 0.55 (threshold)

A minimum and a maximum value are also specified for each parameter (cf table 2).

A footprint on the ground of the sounding elementary pixel is specified between 9 km^2 and 50 km^2.

For a typical diameter of the entrance pupil of 26 mm, a spectral resolving power of 25000 and the mean observation radiance, table 3 gives the modelled radiometric resolution. The latter is the signal to noise ratio (SNR) in the spectrum by the resolution element after binning 50 pixels along the spatial axis (Fig.3). This binning corresponds to a linear length along the ground and at the satellite nadir of 5 km. Integration time is such that the elementary FOV footprint covers 5 km x 5 km.

TABLE II. Specifications of parameter

Spectral bands	B1	B2	B3
BW	50 - 150cm-1	30 - 90cm-1	
SNR	200 - 500		
R	25000 - 42000		
M	≥ 4 along 50 km track trace		
N	1≤ N ≤ 5		

TABLE III. Performances level 1

	B1	B2	B3
Power resolution	25000	25000	25000
Pixels / FWHM	4.8	2.4	2.4
Diffraction order	35	17	13
SNR	270	580	250

The echelle grating is an etched model with 69.33 lines/mm, used with an incidence angle of 67.9°. The effective size of the grating is 48 mm x 140 mm.

In its reference operating mode, the instrument simultaneously acquires five contiguous, independent FOV with the radiometric resolution indicated in table 3. The instrument's ground swath when the slit length is perpendicular to the satellite velocity axis is therefore 25 km. Within this swath, the pixel binning areas can be chosen as needed to avoid cloudy areas.

B. Pseudo-noises (level 1)

Along with the key parameters considered in the important function described above, instrument defects will affect the spectrum measured in the spectral bands, and therefore the precision of the estimated CO2 concentration. Such defects have a similar effect on radiometric noise, which is why the term "pseudo-noise" is used. Different kinds of pseudo-noise include:

- geometric defects such as inter-band and intra-band co-registration…
- spectral defects such as ILS (Instrument Line Shape) knowledge, keystone…
- polarisation defects,
- calibration residue,
- non-linearity and non-uniformity defects,

The goal is to design an instrument for which pseudo-noise is limited and noise mainly consists in radiometric noise.

In the case of non-linearity defects, one of the main contributors is the detector, especially in the low signal dynamic. Let us examine this defect more closely.

In the preliminary study, to reduce development and qualification costs, we used performances of HgCdTe off-the-shelf detectors from Sofradir for B2 and B3 bands to perform our radiometric calculations [5]. The size of the detector is 500x256 pixels, with a 30µm pitch and uses Capacitive TransImpedance Amplifier (CTIA) readout circuit. This choice means that we have to deal with non-customised components. For instance, the capacitance is larger than we need, which induces read-out noise and non-linearity issues.

Existing data concerning detector response show an increase in pixel response dispersion under 10% of full well capacity and a non-linearity shape different from one pixel to another.

It is important to determine whether non-linearity observed at low levels is due to measurement precision, and can be treated as a noise, or if it is a signed response of the CTIA that has to be taken as a bias.

In order to keep to the specified objective of not being dominated by pseudo-noise, the design has been studied to increase the signal (integration time and optics diameter).

C. *Polarisation*

Incident solar radiation at the top of the atmosphere is non-polarised. Two mechanisms polarise it: scattering throughout the atmosphere, and reflection by the surface.

Polarisation by the atmosphere is caused by radiation scattering, particularly Rayleigh scattering (by molecules), as well as scattering by aerosols (the smaller they are, the greater their polarising effect will be). The rate of polarisation by the atmosphere is variable and can be high: especially in absorption lines because of Rayleigh polarisation).

In the case of polarisation by specular-type reflection, the size of the IFOV considered is an important parameter. For kilometric resolution (MICROCARB or POLDER type), the phenomenon of unpolarized lambertian reflection clearly prevails for a view of the nadir on earth. For a view of the sea, however, due to the glint, the polarisation rate can be nearly 100% with low winds (specular surface, see Fresnel's Law), which confirms the signal's potentially high polarisation level when it enters the instrument.

For MicroCarb, the instrumental polarisation is specified so as to ensure that its impact on the signal measured by the detector is negligible compared to the radiometric noise. Other strategies can also be used. The polarisation can be measured by the instrument, for example, which is what the GOSAT instrument does. The measurement can also be taken using fixed polarisation, as in the case of the OCO instrument.

Specifying polarisation with the MicroCarb approach has been established as follows: by rotating the polarisation plane of the polarised monochromatic incident flux, the instrumental polarisation appears as a variation in the recorded signal. In quantitative terms, this leads to specification of the defined polarisation ratio as p=(Imax-Imin)/(Imax+Imin), in which Imax and Imin are the maximum and minimum intensity readings when the polarisation plane is rotated by 180°.

In glint mode: Tp < 0.1% at the goal and 0.7% at the threshold

In nadir mode: Tp < 0.25% at the goal and 5% at the threshold

With these values, considering the expected polarisation rate values for scenes on entry, the pseudo-noise level is below 1:1000.

A component which makes up a considerable share of the overall instrument budget is the grating, and special care is taken to ensure good grating polarisation performance. This is why we have developed a grating polarisation model (see paragraph IV) and studied very precise characterization of instrument polarisation and its main contributing factors. Nevertheless, to meet the required specification level, a polarisation scrambler (optical depolarising component) needs to be inserted in the MicroCarb design.

IV. POLARISATION OF ECHELLE GRATING

A. *Requirements*

It is tricky to find a diffraction Grating with low polarisation and good efficiency, and we know that this will be the main contributor to the instrument polarisation.

As the instrument polarisation requirement is <0.1% we are forced to add a depolariser to the instrument, as this value is out of the state of the art for gratings. But a depolariser only reduces the instrument polarisation; it is thus important that the grating itself should have the lowest possible polarisation.

We are working with both Richardson Gratings and Horiba Jobin Yvon companies to find the best grating for polarisation and efficiency. The different gratings ordered from both will then be mounted on our breadboard and characterized for comparison.

B. *Modelling Polarisation*

A development was made with Institut Fresnel [6] to build a grating model in order to predict grating performances for our instrument.

The model was achieved and compared with real measurements on several different gratings, including gratings with uncommon profiles, and immersed gratings.

The figure 7 shows the comparison for the Richardson Grating (ref 53_*_453E) that we currently use on the MicroCarb Breadboard.

There is a good agreement between performance simulations and measurements, as well as for absolute efficiency and for polarisation. The model is able to take into account real groove profiles, high orders of diffraction, and a high angle of incidence.

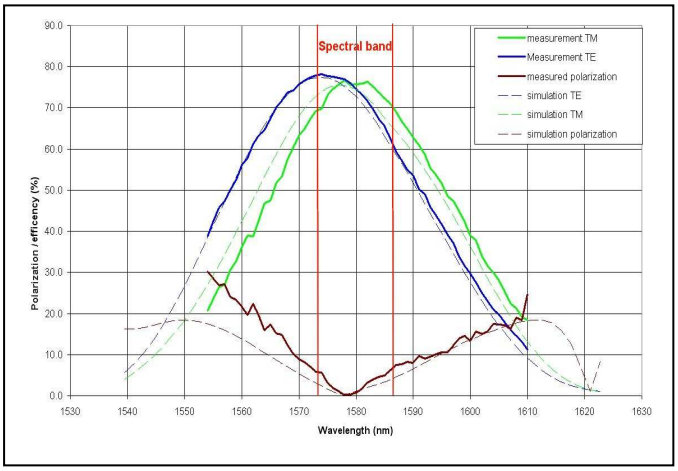

Figure 7. Comparison between grating measurement and simulation using real groove profile. 31.6 grooves/mm, Blaze = 71.45°, diffraction order 38, const deviation = 0.6°

The echelle grating we are currently using on the MicroCarb breadboard has a polarisation under 5% and an efficiency > 65% on a 15 nm spectral range in band B2 (Fig. 7), which is a really good performance. But this echelle grating is not a custom grating, and does not exactly match MicroCarb spectral bands, even if it is close. Thus, through CNES Research and Development program, we are looking for a grating that fulfils the MicroCarb project needs, with both Richardson and Jobin Yvon. We aim at a polarisation under 5% in each of the 3 MicroCarb spectral bands, along with an efficiency above 70%.

C. Measuring efficiciency and polarisation of gratings with breadboard

This part outlines the echelle grating measurement method with the MicroCarb breadboard.

Figure 8 illustrates the measurement of efficiency in band B1. This measurement is made directly with the MicroCarb breadboard. The results are thus fully representative of the grating performance with the instrument conditions (angle of incidence, beam size, wavelengths, order of diffraction…).

A first measurement is made with the echelle grating, and a second measurement with a reference mirror in order to be able to correct the grating measurement from the instrument spectral response.

The measurement is made with a collimated beam in quasi Littrow, with a constant angular deviation of 0.6° (Fig.6). This means that the incidence angle on the grating is adjusted for each wavelength, so that the angular deviation is 0.6°. This is necessary to ensure a rigorous comparison of the measurement with the reference mirror.

A polarizer in the breadboard is used to measure the efficiency under TE or TM polarisation. Figure 8 illustrates the measurement of polarisation in band B2.

The sources are 2 tuneable lasers ([760-780nm] and [1460-1610 nm])

This setup makes it possible to test and compare many different gratings, and to use real measurements in the instrument simulator.

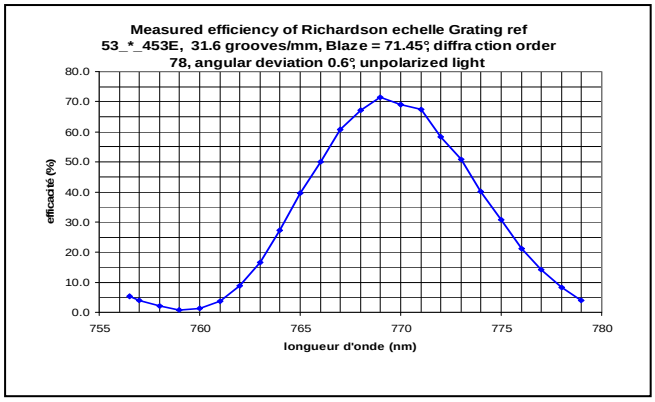

Figure 8. Example of spectral response of Richardson echelle gratings measured with the breadbord in band B1

V. INSTRUMENT SIMULATOR

A. Description of the instrument simulator

Calculating the performance of a spectrometer is fairly complex and requires modelling of various types of instrumental defects (spectral, electronic, spatial, etc.) as well as a calibration strategy. A model of the dispersive spectrometer as described in Figure 4. physics equations, can be used to obtain the signals measured on the detection matrix (science measurements and calibration measurements) using a sun spectrum, atmospheric spectrum or specific sources (blackbody, gas cell, laser…). The instrumental defects from the optical, detection or electronic systems, etc. are then added. The kinds of defects typically encountered include:

- Image quality and geometric defects caused by grating/slit, grating/detector misalignments, etc.
- Spectral defects introduced by optics (Smile or Keystone type), deformation of the slit projection on the detection matrix.
- Spectral response defects, from the filters or the detector, which offset or deform the spectral response for each detector pixel.
- Spatial instrument defects (offsets, interpixel gain, non-linearity type defects, etc.)
- Radiometric noise (photonic or other kinds of noise).
- Polarisation residue

This way, we can model the level 0 measured by the instrument and level 1. Level 0 corresponds to non-calibrated raw digital signals picked up as they exit the detection lines. All of the raw measurements will be used to check level 1 products, calibrated spectral products. Setting up an instrument modelling software programme has proved usefulness in establishing or verifying the validity of the instrument specification.

The flow diagram for the MicroCarb instrument model is presented in Fig. 9.

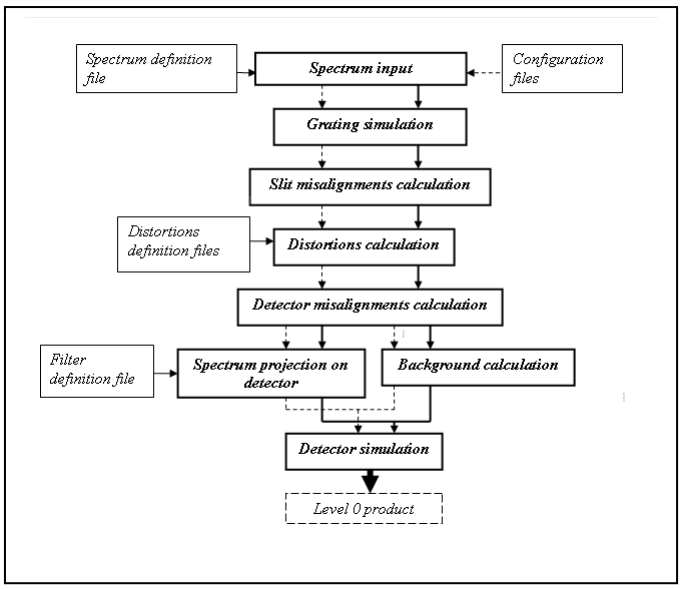

Figure 9 Flow diagram for the MicroCarb instrument model

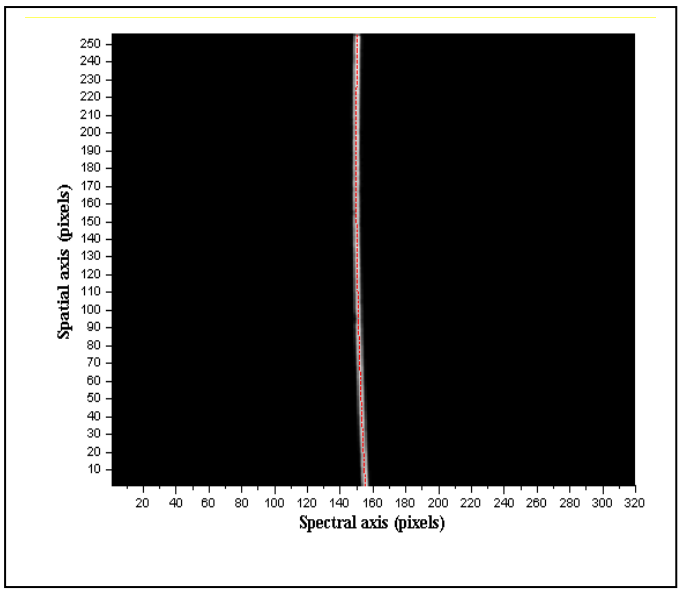

Figure 10 Estimated distortion on the image obtained using the laser

B. Illustration with breadboard simulation

The characteristics of the specific MicroCarb mock-up set out in paragraph II above have been taken into account in the instrument simulator.

Since there is a slit image projection for each wavelength, by using the slit defects and studying their position in the field when they are projected on the detector, we are able to estimate the misalignment of the optics. This way, we have been able to estimate certain defects more precisely:

- misalignment of optics
- distortion of the mock-up optics.

After correcting the misalignment, we proceed to estimate the optical distortion.

The image of a laser line through the spectrometer is distorted by the optics. To evaluate this, we calculate the barycentre of the laser line as a function of the position in the field (spatial axis), and we then make this curve a fit curve. This gives us the distortion associated with the wavelength of the laser line (Fig. 10).

Using the results of the measurements taken with the mock-up (laser line spectrum at 770nm, Fig.10), the shape of the line on the detector was estimated as illustrated in Figure 11.

For this estimation, we correct the distortion and then combine the spectrums from different positions in the field in order to obtain the average shape.

The shape above corresponds to a resolution power of 31000. A supergaussian shape of around 1.6 fits best with the shape's reconstruction.

The dispersion seen here is due to the presence of speckles relating to the use of a laser source for the measurement, rather than the instrument itself. Some improvements are in progress on the breadboard to reduce these speckles.

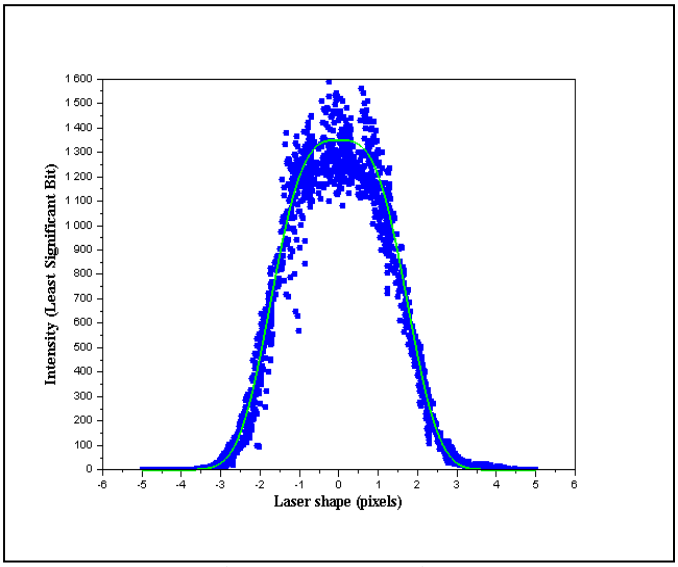

Figure 11: Example of the measured shape of a laser line (dots) and the modelled shape (continuous line).

VI. Conclusion

To fulfill the objective performances/achievements of the spectrometer in the range of MicroCarb, a special attention must be brought for reducing the pseudo noise as in particular the non linearity defects and the polarisation defects.

Concerning the non linearity, at low signal; the detector tends to be the main contributor. Using the existing HgCdTe detectors from Sofradir led us to find an operating point that allows to use them above 10% of charge handling capacity in order to guaranty linearity. Another solution may be to use a SFD (Source Follower per Detector) readout circuit well suited for low levels, a specific R&D is in progress with CEA/Leti and Sofradir on this subject.

Concerning the polarisation, the requirement below 0.1% is very challenging and this can be reached thanks to an effort on the major contributing grating and thanks to the integration of a scrambler in the design. A modeling and characterization study was set up to be capable of predicting the performance that will be reachable according to the grating design. This work was presented for echelle gratings and is in progress with immersed grating.

In order to understand the impact of these technological components on the performances, an instrument simulator was set up for the MicroCarb project. Linking the instrument simulator with the breadboard is very interesting to validate the concept performances.

This compact design approach combined with the Myriade Evolution product line will allow CNES to offer a low-cost solution for the mission purposes. This solution will pave the way for operational long-term CO_2 monitoring from a constellation of microsatellites.

The original CNES phase 0 study presented in this paper has been a basis for the current industrial phase A. The breadboard and the instrument simulator get additional expertise on performances and technological components.

More information can be found on the CNES website http://microcarb-mission.cnes.fr

References

[1] R.Haring, R.Pollock, B.M.Sutin, and D.Crisp,The Orbiting Carbon Observatory instrument optical design, Proc SPIE 5523, 51-62, 2004

[2] C.Buil, V.Pascal, J. Loesel, C. Pierangelo, L.Roucayrol, L. Tauziede, A new space instrument concept for the measurement of CO2 concentration in the atmosphere, SPIE 8176-12 Remote Sensing Europe, Prague, 2011

[3] Annmarie Eldering, Benjamin Solish, Peter Kahn, Stacey Boland, David Crisp, Michael Gunson, High Precision Atmospheric CO2 Measurements from Space: The Design and Implementation of OCO-2, Proceedings of the 2012 IEEE Aerospace Conference, Big Sky, Montana, USA, March 3-10, 2012

[4] C D Rodgers, Inverse Methods for Atmospheric Sounding Theory and Practice, WorldSci, Singapore, 2000

[5] YR. Nowicki-Bringuier, P. Chorier, Sofradir SWIR hyperspectral detectors for space applications, Sensors, Systems, and Next-Generation Satellites XIII. Edited by Meynart, Roland; Neeck, Steven P.; Shimoda, Haruhisa. Proceedings of the SPIE, Volume 7474 (2009)., pp. 747417-747417-12, 2009

[6] E. Loewen, D. Maystre, E. Popov, and L. Tsonev, Echelles: scalar, electromagnetic, and real groove properties 1 April 1995 @ Vol. 34, No. 10 @ APPLIED OPTICS 1707-1727